tumors. However, as the antitumor immune response is based on the balance between the effector and regulatory sides of immune cells; the decrease of Treg ratio (Figure 7d) and inhibition of Treg activity (Figure 7b) may lead to a strong antitumor immunity.

DISCUSSION

In this study, we showed that an intratumoral *IFN-α* gene transfer significantly enhances a systemic tumor-specific immunity in the synHSCT recipients. The precise mechanism for the enhancement is

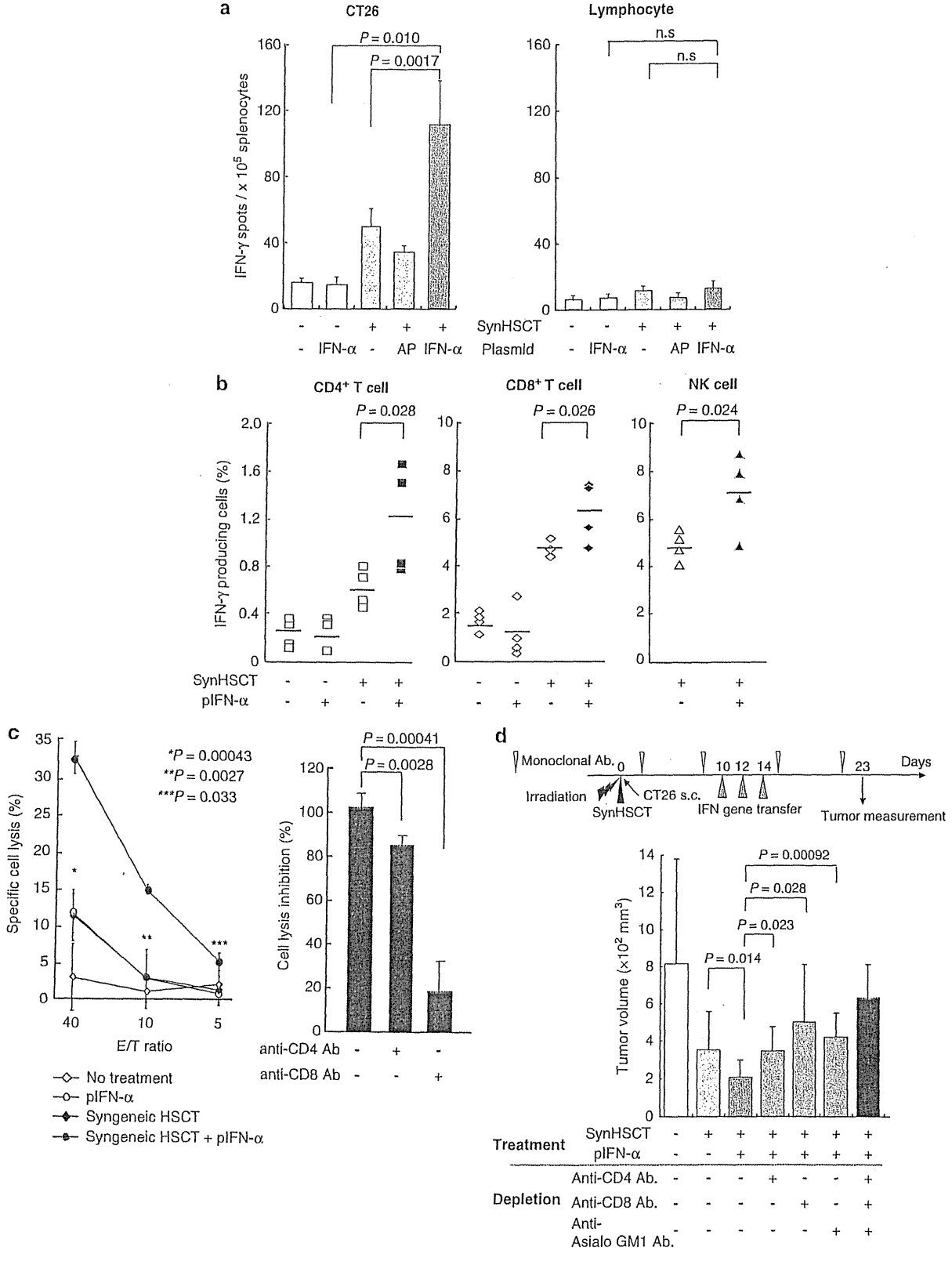

not completely understood, but it should include an effective stimulation of DCs by the expression of IFN-α in the tumors in synHSCT recipients, because (1) intratumoral expression of IFN-α effectively induces cell death of cancer cells and exposes TAAs in large quantity to DCs ($CD11c^+$ cells);[12] (2) IFN-α promotes maturation of $CD11c^+$ cells, which facilitates the presentation of TAAs on $CD11c^+$ cells (Figure 6a); (3) $CD11c^+$ cells in the tumors transduced with the *IFN-α* gene produce a large quantity of immune-stimulatory cytokines such as IL-12 (Figure 6b); (4) the $CD11c^+$ cells in the treated tumors suppress the inhibitory activity of Tregs (Figure 7b). The combination of immune-stimulatory effects by IFN-α and the reconstitution of a fresh immune system following HSCT could create an environment strongly supporting the activation of an antitumor response. We propose a model showing the integrated mechanisms of inducing a strong antitumor immunity by a combination therapy (Figure 8).

Although the conditioning of HSCT with irradiation and/or immunosuppressive reagents can destroy the immunotolerance deployed by the tumor, the tumors restore a tolerant microenvironment by induction of Tregs and the production of immune-inhibitory cytokines,[18] which may be one of the main reasons for the failure to fully sustain HP-mediated antitumor immunity. An analysis of the cytokine profile unexpectedly showed that the IFN/HSCT-$CD11c^+$ cells produce a large amount of IL-6 as well as other immune-stimulatory cytokines (Figure 6b). It has been reported that IL-6 increases methylation of upstream Foxp3 enhancer and represses the Foxp3 transcription in natural Tregs.[19] Our findings demonstrated that $CD11c^+$ cells isolated from the tumors transduced by *IFN-α* gene significantly suppress the activity of Tregs (Figure 7b), which may inhibit or delay the reconstitution of an immunotolerant microenvironment in the tumor. $CD11c^+$ cells seem to have a capacity to produce IL-6 in response to IFN-α in a dose-dependent manner (Figure 7a). The IL-6 production was increased in the HSCT-$CD11c^+$ cells also (Figures 6b and 7b). The intratumoral IFN-α expression and the immune-stimulatory condition by elevated cytokine levels after synHSCT may synergistically influence $CD11c^+$ cells to produce IL-6. It is also reported that IL-6 promotes carcinogenesis through multiple signal pathways.[20] The role of IL-6 in tumors is probably based on the balance between the positive and negative effect of IL-6 on the tumor growth. Although it is known that DCs secrete proinflammatory cytokines such as IL-6 by toll-like receptor stimulation,[17] further research is needed to clarify the critical factor/pathway for the production of IL-6 from DCs in synHSCT recipients.

As HP leads to a break in tolerance against self-antigens, the expression of IFN-α could theoretically promote T-cell response not only against tumor cells but also against host normal cells, which may cause an autoimmune reaction. However, no overt toxicity was observed for the treated mice, including their blood chemistry. The immunogenic DCs at the IFN-α vector-injected tumor site were able to capture both TAAs and normal self-antigens shared by tumor and normal cells, and promote tumor-specific immunity and a local autoimmune reaction, whereas resting host DCs away from the tumor site present only normal self-antigens and may induce tolerance or exhaustion of host-reactive T cells. Alternatively, we recently found that the percentage of $Foxp3^+$ cells per $CD4^+$ T cells in the spleen was clearly elevated at an early phase after syngeneic HSCT (data not shown), which differed from the low frequency of $Foxp3^+$ T cells in the tumor (Figure 7d). The finding suggests that among $CD4^+$ T cells, Tregs rapidly proliferate during HP in the body, which might protect patients against autoimmunity after autologous HSCT.

There have been several animal studies showing the potential efficacy of gene- and cell-based immunotherapy in syngeneic HSCT mice. The vaccination with syngeneic tumor cells expressing granulocyte-macrophage colony stimulating factor showed a strong antitumor effect in the transplanted mice.[5] An immunization with DCs pulsed with whole tumor cell lysates led to efficient antitumor responses in a mouse breast tumor model.[21] Adoptive transfer of tumor-specific T cells has also shown enhanced antitumor immune responses after HSCT in lymphopenic mice,[2] and recently, Morgan *et al.*[22] reported efficacy of a strategy composed of immunodepletion and adaptive cell transfer for patients with metastatic melanoma. As tumor-reactive T cells are mostly polyclonal, and heterogeneous expressions of various TAAs coexist even in a tumor mass, the *in vivo* stimulation of multiple tumor-reactive lymphocytes might be critical in the clinical application. Moreover, compared with the previous approaches, another major advantage of an *in vivo IFN-α* gene transfer is that it does not involve a manipulation and culture of the immune and tumor cells *ex vivo*, making this strategy more feasible for many patients with solid cancers. We previously reported that an allogeneic MHC gene transfer also could enhance an effective antitumor immunity in HSCT recipients.[6] The major difference between the allogeneic MHC and *IFN-α* gene therapies is in their local effects on tumor sites transduced with the therapeutic genes: *IFN-α* gene transfer significantly induces cell death and growth inhibition (Figure 2b and see Hara *et al.*[12]). In addition, IFN-α seems to have direct effects upon DCs such as the maturation of the cells and production of immune-stimulatory cytokines and enhancement of inhibitory activity against Tregs. Therefore, a local *IFN-α* gene therapy is a promising therapeutic strategy, especially in a case in which cancer conditions need strong local tumor control and systemic antitumor activity.

Some of the experiments in this study showed important points to consider in the clinical feasibility of the combination therapy.

Figure 4 A large number of IFN-α-producing cells are induced by intratumoral *IFN-α* gene transfer in synHSCT recipient mice. (**a**) Enzyme-linked immunosorbent spot assay of IFN-γ-producing cells in response to stimulation of CT26 cells. At 2 weeks after plasmid-mediated *IFN-α* gene transfer, mouse splenocytes were isolated from treated mice and co-cultured with CT26 cells or control lymphocytes (n=3). The experiments were repeated three times. (**b**) Intracellular cytokine staining of IFN-γ-producing cells in response to stimulation of CT26 cells. The splenocytes (1×10^6) from treated mice were incubated with CT26 (1×10^5) and stained by allophycocyanin-anti-mouse IFN-γ. The activated cell fractions were analyzed by staining with fluorescein isothiocyanate-anti-mouse CD4, CD8 or CD49b (labeling NK cell) antibody (n=3–4). The experiments were repeated twice. (**c**) *In vitro* cytotoxic assay of splenocytes. Splenocytes were isolated from the treated mice, and their cytotoxicity was evaluated in a standard 4 h ^{51}Cr release assay against CT26 cells (n=3). The statistical difference between cell lysis in the synHSCT mice with *IFN-α* gene transfer and synHSCT alone mice is presented (left panel). Splenocytes isolated from synHSCT mice with *IFN-α* gene transfer were pre-incubated with the anti-CD4 or anti-CD8 antibodies for 1 h before cytolysis for CT26 cells (right panel). The data are expressed as cell lysis inhibition (%) at E/T ratio=40 (cell lysis with co-incubation of antibody/that with no antibody). The experiments were repeated twice. (**d**) Antitumor effect of *IFN-α* gene transfer after *in vivo* depletion of $CD4^+$ T cells, $CD8^+$ T cells and NK cells. A group of transplanted mice were treated with anti-CD4, anti-CD8 or anti-asialo GM1 antibodies (targeting NK cells) to deplete these cell populations, and the CT26 tumors were injected with pIFN-α vector (n=7–9). Tumor volumes at 10 days after *IFN-α* gene transfer are presented.

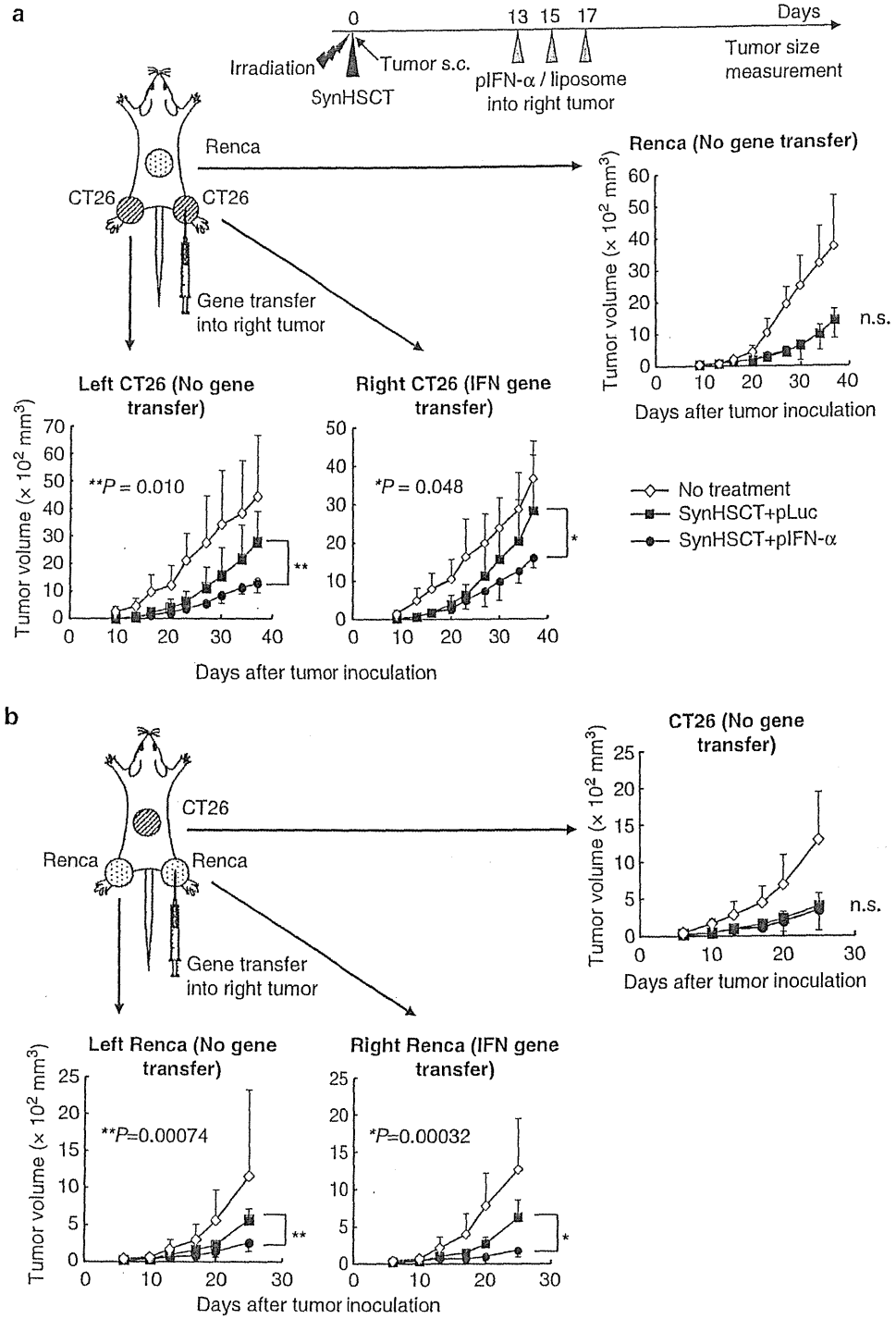

Figure 5 Suppression of tumors at distant site by *IFN-α* gene transfer during immune reconstitution. The experiments were repeated two times. (a) Intratumoral *IFN-α* gene transfer into CT26 tumors. CT26 cells were inoculated on both legs and Renca cells were inoculated on the back in synHSCT mice. The pIFN-α/liposome complex was injected into CT26 subcutaneous tumors on the right legs at days 13, 15 and 17 (n=4–8). (b) Intratumoral *IFN-α* gene transfer into Renca tumors. Renca cells were inoculated on both legs and CT26 cells on the back in synHSCT mice. The pIFN-α/liposome complex was injected into Renca subcutaneous tumors on the right legs at days 13, 15 and 17 (n=4–8). (c) Suppression of liver metastasis. CT26-Luc cells were injected beneath the splenic capsule to generate liver metastasis, and CT26 cells were inoculated on the right leg. After the *IFN-α* gene transfer, the size of subcutaneous tumors on the legs was macroscopically measured, and photon count of abdominal tumors was evaluated by the IVIS imaging system. (d) *Ex vivo* imaging of the liver. The livers were resected from treated mice at 21 days after the synHSCT, and photon spots and counts of the livers were evaluated by the imaging system. Arrowheads: liver tumors.

First, a liposome-mediated *IFN-α* gene transfer effectively suppressed tumor growth in synHSCT recipients. Although the peak level of IFN-α expression was not very high, the expression continued for more than 10 days after gene transfer (Figure 2d), suggesting that a high concentration of IFN-α in the tumors is not necessary and that the continuous expression is important to induce an effective antitumor

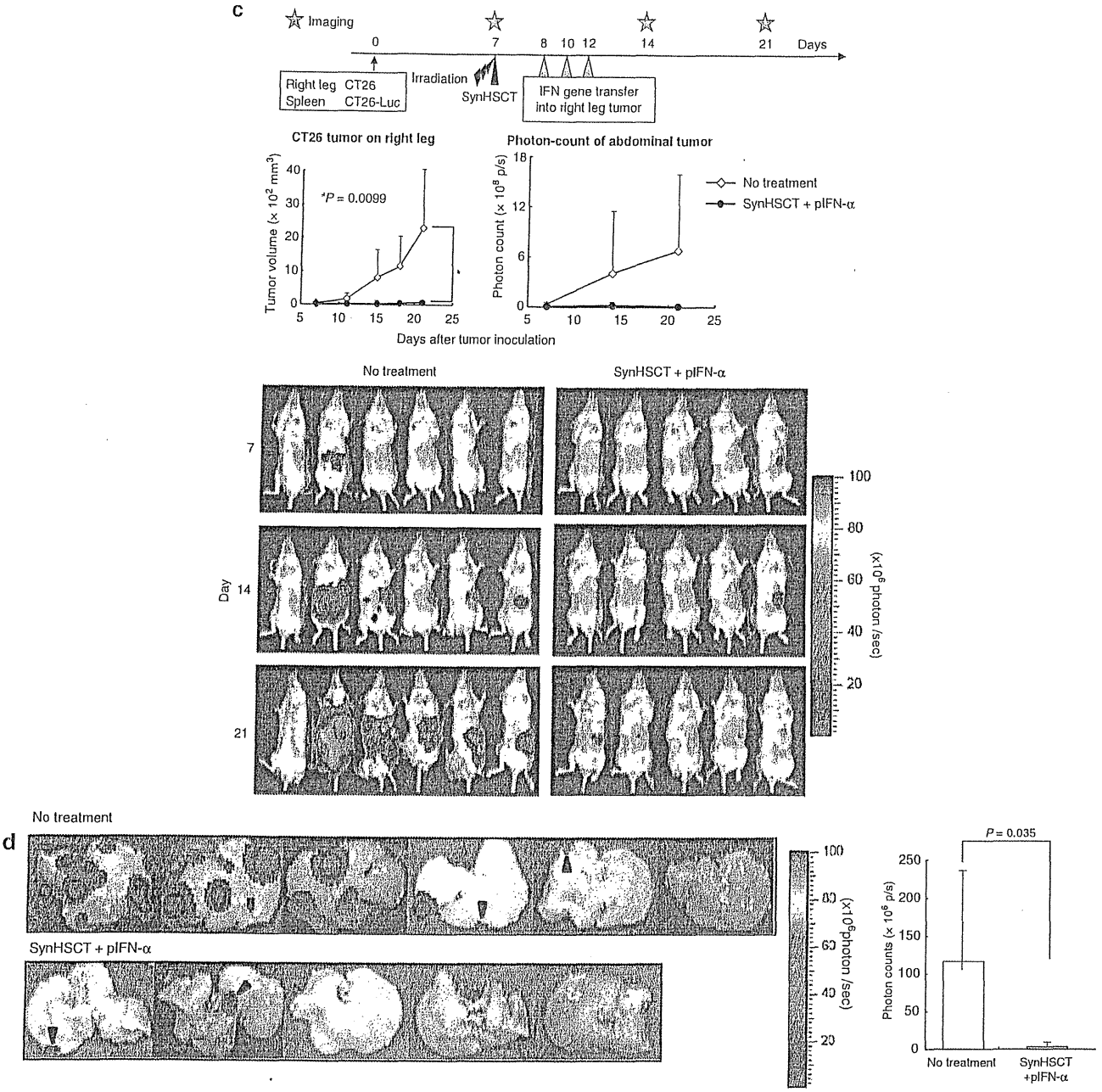

Figure 5 Continued.

immunity. This facilitates a clinical application, because *in vivo* lipofection of an IFN-α-expressing plasmid is much safer than virus vectors, although the latter has a high gene transduction efficacy.[14] Second, the intratumoral *IFN-α* gene transfer at 6 weeks after synHSCT significantly suppressed tumor growth and prolonged the survival of synHSCT mice (Figures 2e and f). At 6 weeks after synHSCT, neutrophil count returned to a normal level (data not shown), which avoids the risk of bacterial infection that accompanies a needle injection for intratumoral gene transfer. Third, a combination therapy was effective in suppressing not only the vector-injected tumors but also the vector-uninjected distant tumors in the liver metastasis model, which resembles a clinical setting. The results indicated that this treatment strategy might be feasible for many patients with solid cancers. The next step in research may include a further elucidation of the main mechanism of IFN-α in inducing tumor immunity and the synergism between IFN-α and synHSCT, including identification of potential key factors other than IL-6 and DC, development of methods to further sustain and control tumor-specific immunity and to predict and monitor HP followed by an individualization of the combination therapy.

In conclusion, a combination of intratumoral *IFN-α* gene transfer with synHSCT is a promising immunotherapy for solid cancers, because of the activation of tumor-specific immunity, suppression of the immunotolerant environment and excellent safety features. This therapeutic strategy deserves an evaluation in future clinical trial for solid cancers.

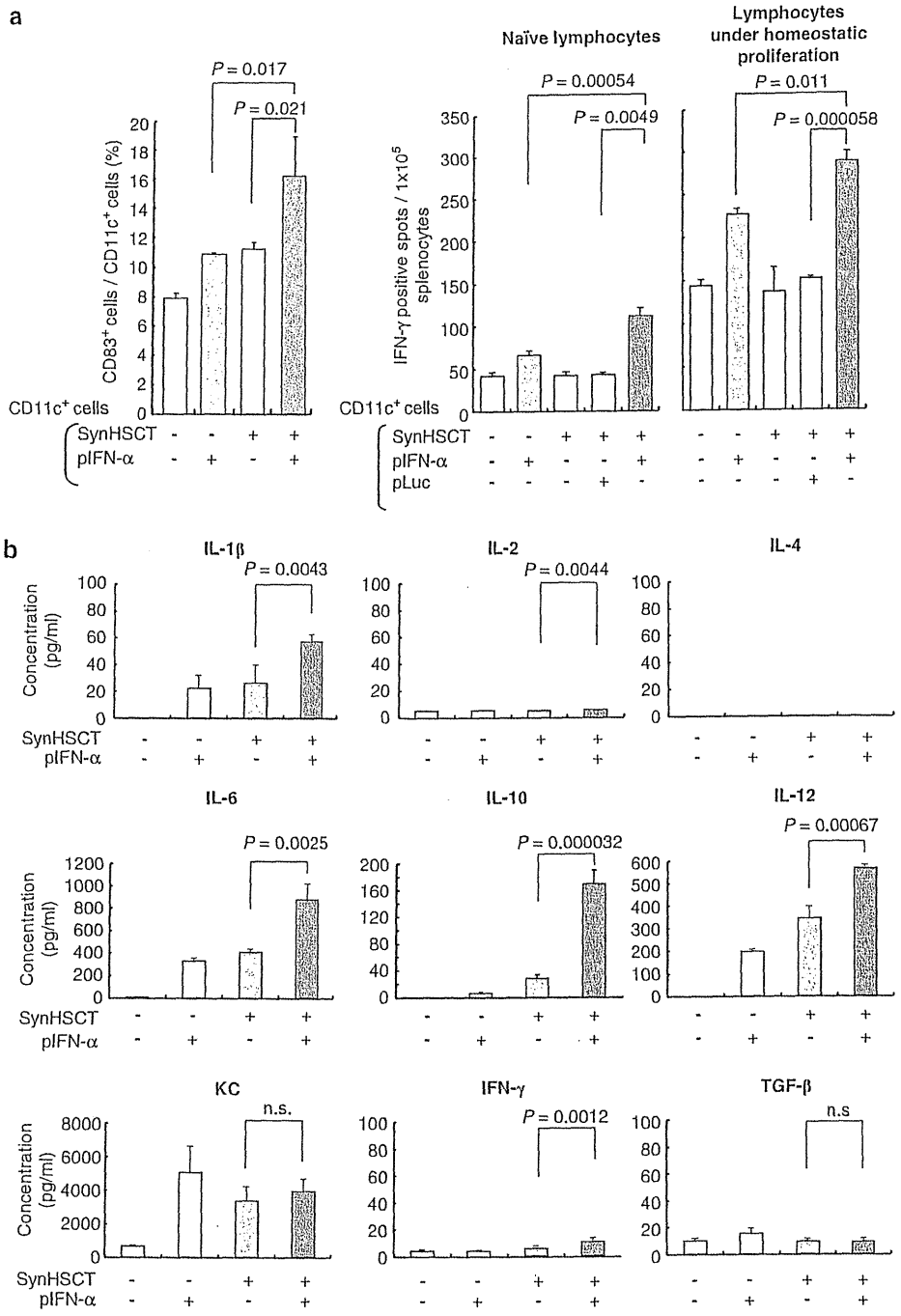

Figure 6 IFN-α expression promotes the maturation of CD11c$^+$ cells in the tumor. (**a**) Number of IFN-γ-positive cells by enzyme-linked immunosorbent spot assay. Flow cytometry of CD83$^+$ cells (Michel-19; BD Pharmingen) was performed in the CD11c$^+$ cells isolated from tumors (n=3). The frequency of CD83$^+$ cells per CD11c$^+$ cells is presented (left panel). CD11c$^+$ cells from treated tumors were co-cultured with lymphocytes isolated from naïve BALB/c mice (middle panel) or synHSCT mice (right panel), and lymphocyte activation was measured by IFN-γ-enzyme-linked immunosorbent spot assay (n=3). The experiments were repeated twice. (**b**) Cytokine production of CD11c$^+$ cells. CD11c$^+$ cells were isolated from treated tumors (n=3), and were seeded in a 48-well plate (1×10^5 cells per well). After the incubation for 48h, cytokines in the medium were measured by a cytokine array (Procarta Cytokine Assay Kit; Panomics, Inc., Fremont, CA, USA). IL-10 level was measured by enzyme-linked immunosorbent assay (Quantikine; R&D Systems, Minneapolis, MN, USA). The experiments were repeated three times.

MATERIALS AND METHODS

Animals and hematopoietic stem cell transplantation

Seven-to-nine-week-old female BALB/c (H-2^d Ly-1.2) mice were purchased from Charles River Japan, Inc., (Kanagawa, Japan). Animal studies were carried out according to the *Guideline for Animal Experiments of the National Cancer Center Research Institute* and approved by the Institutional Committee for Ethics in Animal Experimentation. Nine-to-ten-week-old BALB/c mice received a lethal (9 Gy) irradiation on the day of transplantation. The irradiated BALB/c mice were injected intravenously with 5×10^6 of bone marrow cells and 2×10^6 splenic T cells from donor BALB/c mice. Bone marrow cells were isolated from donors by

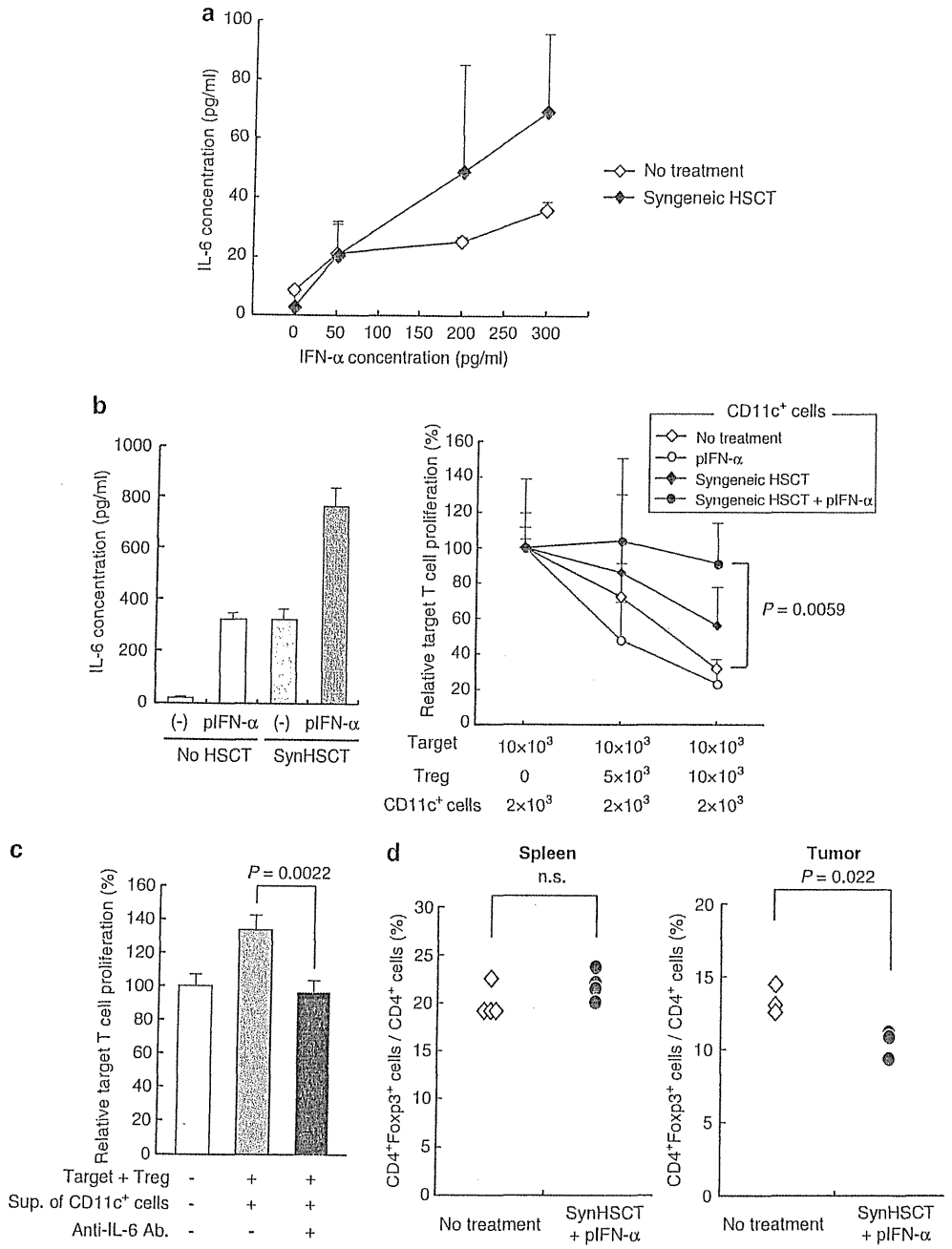

Figure 7 CD11c$^+$ cells in the tumor inhibit the immunosuppressive activity of Tregs. (**a**) CD11c$^+$ cells produce IL-6 in response to IFN-α. CD11c$^+$ cells isolated from the spleens of non-HSCT and synHSCT tumor-bearing BALB/c mice were seeded in a 96-well plate (1.5×10^5 cells per well) and cultured in the medium containing IFN-α protein at indicated concentration for 2 h. After the change of medium, the cells were incubated for 48 h, and IL-6 in the medium was measured by ELISA (Quantikine; R&D Systems). The experiments were repeated twice. (**b**) The inhibition of activity of Tregs by CD11c$^+$ cells. The CD11c$^+$ cells were isolated from treated tumors and seeded in a 48-well plate (1×10^5 cells per well), and after incubation for 24 h (n=4) (left panel), IL-6 production from the CD11c$^+$ cells was measured by ELISA. Target cells (CD4$^+$CD25$^-$ T cell) and Treg (CD4$^+$CD25$^+$ T cell) were isolated from the spleen of naïve BALB/c mice, and were co-cultured with the designated CD11c$^+$ cells in a CD3-coated 96-well plate, and the proliferation of target cells was examined by ^{3}H-thymidine uptake assay (n=3) (right panel). The experiments were repeated three times. (**c**) IL-6-mediated suppression of Treg activity. Target cells and Tregs were cultured in a CD3-coated 96-well plate with the supernatant of CD11c$^+$cells from treated tumors, and the proliferation of target cells was evaluated by ^{3}H-thymidine uptake assay (n=3). The addition of anti-IL-6 antibody (R&D systems) was used to neutralize mouse IL-6 in the medium. The experiments were repeated twice. (**d**) The frequency of Tregs in the spleen and treated tumors. The lymphocytes were collected from the spleens (n=4, left panel) and treated tumor (n=3, right panel), and Foxp3$^+$ and CD4$^+$ cells were analyzed by flow cytometry.

flushing each femur and tibia with RPMI-1640 medium (RPMI) supplemented with 5% heat-inactivated fetal bovine serum (ICN Biomedicals, Inc., Irvine, CA, USA), and splenic cells were prepared by macerating the spleens. After lysis of the erythrocytes, splenic cells were incubated with anti-Thy-1.2 immunomagnetic beads (Miltenyi Biotec GmbH, Bergisch Gladbach, Germany) at 4 °C for 15 min, followed by selection of T cells by AutoMACS (Miltenyi Biotec).

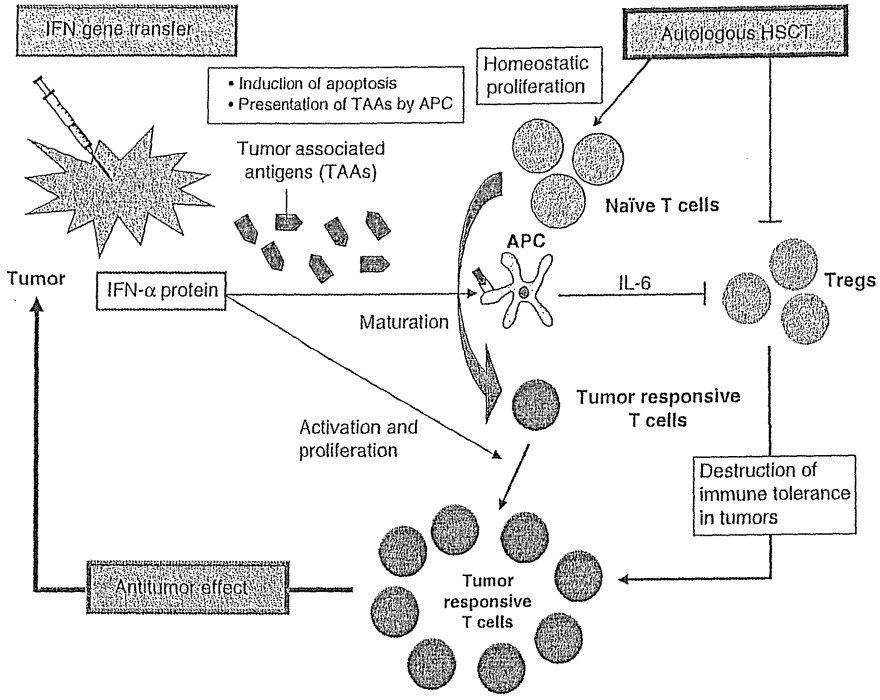

Figure 8 Model showing integrated mechanisms of inducing strong tumor immunity by a combination therapy. In the 'homeostatic proliferation' condition after synHSCT, T cells effectively recognize the low-affinity self-antigen including TAAs, leading to an induction of antitumor immunity. The conditioning of HSCT with irradiation and/or immunosuppressive reagents can destroy the immunotolerance mechanisms developed by the tumor. Furthermore, IFN-α expression in the tumors exposes TAAs in large quantity to DCs, and IFN-α promotes maturation and enhances the antigen-presenting capacity of DCs. In addition, DCs produced a significant amount of IL-6 in response to IFN-α, which suppress the proliferation and activity of Tregs. The integrated mechanisms are capable of inducing a strong antitumor immunity against solid cancers.

Tumor cell lines, recombinant adenovirus vectors and plasmid vectors

CT26 and Renca (American Type Culture Collection, Rockville, MD, USA) are weakly immunogenic BALB/c-derived colon and renal cancer cell lines, respectively. Cells were maintained in RPMI containing 10% fetal bovine serum, 2 mM L-glutamine and 0.15% sodium bicarbonate (complete RPMI). A CT26 cell line that stably expresses the firefly luciferase gene was generated by retrovirus vector-mediated transduction and designated as CT26-Luc. The recombinant adenovirus vectors expressing mouse interferon-α (Ad-mIFN) and alkaline phosphatase cDNA (Ad-AP) were prepared as described.[23,24] The recombinant adenoviruses are based on serotype 5 with deletions of the entire E1 and a part of the E3 regions, and have the CAG promoter, which is a hybrid of the cytomegalovirus immediate early enhancer sequence and the chicken β-actin/rabbit β-globin promoter. A cesium chloride-purified virus was desalted using a sterile Bio-Gel P-6 DG chromatography column (Econopac DG 10; Bio-Rad, Hercules, CA, USA) and diluted for storage in a 13% glycerol/phosphate-buffered saline solution. All viral preparations were confirmed by PCR assay to be free of $E1^+$ adenovirus. A plasmid DNA (pIFN-α) expressing the *IFN-α* gene under the control of the CAG promoter was also used for intratumoral gene transfer. The plasmids that express an alkaline phosphatase (pAP) or luciferase gene (pLuc) were used as a negative control.

In vitro cell proliferation assay

Cultured cells were seeded at 2×10^3 per well in 96-well plates and plasmid DNA-liposome (Lipofectamine2000; Invitrogen, Carlsbad, CA, USA) complex was added according to the manufacturer's protocol. The cell numbers were assessed by a colorimetric cell viability assay using a water-soluble tetrazolium salt (Tetracolor One; Seikagaku Corp., Tokyo, Japan) at 5 days after the transfection. Absorbance was determined by spectrophotometry using a wavelength of 450 nm with 595 nm as a reference. The assays (carried out in four wells) were repeated three times.

In vivo tumor inoculation and *IFN-α* gene transfer

CT26 cells (1×10^6) or Renca cells (5×10^6) were injected subcutaneously into the leg of BALB/c mice. When the subcutaneous tumor was established (~0.6 cm in diameter), it was injected once with 50 μl of Ad-mIFN or control vector (Ad-AP). Plasmid DNA–liposome complex was prepared by the addition of 30 μg plasmid DNA into a total of 75 μl phosphate-buffered saline per mouse, followed by the addition of 75 μl of 0.15 mmol l^{-1} DMRIE-DOPE ((+/–)-*N*-(2-hydroxyethyl)-*N*, *N*-dimethyl –2,3-bis(tetradecyloxy)-1-propanaminium bromide/dioleoylphosphatidylethanolamine), which was provided from Vical, Inc., (San Diego, CA, USA). The mixture solution was incubated at room temperature for 15 min, and then injected directly into the tumor three times every other day. The shortest (r) and longest (l) tumor diameters were measured at indicated days and the tumor volume was determined as $r^2l/2$. Data are presented as mean ± s.d. The experiments were repeated two times.

Enzyme-linked immunosorbent spot assays

IFN-γ ELISpot kit (BD Bioscience, San Jose, CA, USA) was used according to the manufacturer's instructions. Briefly, splenocytes (1×10^5) and mitomycin C-treated tumor cells (1×10^4) were co-cultured in 96-well plates pre-coated with mouse IFN-γ (BD Bioscience) for 20 h at 37 °C in complete RPMI medium in triplicate. After washing the wells, biotinylated anti-mouse IFN-γ antibody (2 μg ml^{-1}) was added and incubated for 2 h at room temperature. Then, a streptavidin-horseradish peroxidase solution was added and incubated for 1 h at room temperature. After the addition of an aminoethyl carbozole substrate solution, spots were counted under a stereomicroscope.

Flow cytometry of cell surface marker and intracellular cytokine staining

Allo-phycocyanin-conjugated monoclonal antibody (mAb) to identify mouse IFN-γ and fluorescein isothiocyanate-conjugated mAb to detect CD4, CD8 and CD49b were purchased from BD Pharmingen (San Jose, CA, USA). Splenocytes (1×10^6) were incubated with medium alone (control) or CT26 (1×10^5) cells

for 2 days; brefeldin-A (10 μg ml^{-1}) was then added for 2 h of incubation. After washing, cells were incubated with the CD4, CD8 or CD49b mAbs in a total volume of 100 μl phosphate-buffered saline with 5% fetal bovine serum for 30 min at 4 °C, and then fixed and permeabilized with a permeabilization buffer (BD Biosciences). Cells were finally stained with antibody to IFN-γ for 15 min at room temperature, washed again and analyzed by FACSCalibur (BD Biosciences). Irrelevant immunoglobulin G mAbs were used as a negative control. Ten thousand live events were acquired for analysis.

Cytotoxic assays

An *in vitro* cytotoxic assay was performed as previously described.[12] Briefly, splenocytes were cultured for 4 days with mitomycin C-treated CT26 stimulators, and then the responder cells were collected and used as effector cells. CT26 target cells were labeled with ^{51}Cr (Perkin-Elmer Japan Co., Kanagawa, Japan). For a 4 h chromium release assay, 4×10^5, 1×10^5 and 5×10^4 effector cells were mixed with 1×10^4 target cells in a 96-well round-bottom plate (Corning Incorporated, New York, NY, USA). To evaluate the relative contributions of CD4$^+$ and CD8$^+$ T cells for the tumor cell lysis, effector cells were incubated with mAbs against mouse CD4 (L3L4; BD Pharmingen) or CD8 (Ly-2; BD Pharmingen) for 1 h at 37 °C before mixing with target cells. Supernatants were harvested and counted in a gamma counter (Packard Bioscience Company, Meriden, CT, USA). The percentage of cytotoxicity was calculated as ((experimental c.p.m.–spontaneous c.p.m.)/(maximum c.p.m.–spontaneous c.p.m.))×100. Each assay was carried out in triplicate.

Immunohistochemistry

Immunostaining was performed using streptavidin-biotin-peroxidase complex techniques (Nichirei, Tokyo, Japan). Consecutive cryostat tissue sections (6 μm) were mounted on glass slides and fixed in 99.5% ethanol for 20 min. After blocking with normal rat serum, the sections were stained with rat anti-mouse CD4 and CD8 antibodies (BD Pharmingen). Parallel negative controls with antibodies of the same isotype were examined in all cases. The sections were counter-stained with methyl green.

In vivo depletion of T and NK cells

To deplete the subsets of immune effector cells before and during the treatment with *IFN-α* gene transfer, the synHSCT mice received intraperitoneal injections of 0.3 mg. Monoclonal antibody from the anti-CD4$^+$ hybridoma (clone GK1.5, rat IgG2b) or 1.5 mg mAb from the anti-CD8$^+$ hybridoma (clone Lyt–2.1, mouse IgG2b; see Nakayama and Uenaka[25]) or 0.5 mg of anti-asialo GM1 antibody (targeting NK cells: Wako Pure Chemical Industries, Ltd, Tokyo,. Japan). Administration of antibodies started at 2 days after the inoculation of CT26 cells, and the injection was repeated every 5–6 days, throughout the entire experimental period. Flow cytometry showed that ~80% of CD4$^+$, ~60% of CD8$^+$ T cells and ~80% of NK cells were depleted in the Ab-treated mice.

In vivo imaging of the tumors in a liver-metastasis model

CT26-Luc cells were injected beneath the splenic capsule to generate liver metastasis. The BALB/c mice with CT26-Luc tumors were administered with D-luciferin (150 mg kg^{-1}) (Wako Pure Chemical Industries) by intraperitoneal injection. At 10 min later, photons from animal whole bodies were counted using an *in vivo* imaging system.

Isolation of CD11c+ cells and T-cell proliferation assay

Dendritic cells were isolated using mouse CD11c MicroBeads and AutoMACS magnetic sorter (Miltenyi Biotec) from tumors of non-HSCT mice treated by intratumoral *IFN-α* gene transfer, tumors of synHSCT mice injected with control plasmid and tumors of synHSCT mice treated by intratumoral *IFN-α* gene transfer, and designated as IFN-CD11c$^+$, HSCT-CD11c$^+$ and IFN/HSCT-CD11c$^+$, respectively. The flow cytometry showed that ~90% of isolated cells express CD11c, and that ~80% of the isolated CD11c$^+$ cells are negative for CD14 (macrophage marker), suggesting that a major population of isolated CD11c$^+$ cells is DCs. CD4$^+$CD25$^+$ or CD4$^+$CD25$^-$ T cells were isolated from the spleen of naïve BALB/c mice using mouse CD4 pre-enrichment kit, mouse CD25 selection kit and RoboSep magnetic sorter (StemCell Technologies, Vancouver, BC, Canada). These populations were stained with anti-Foxp3 antibody, and flow cytometry revealed that about 80% of CD4$^+$CD25$^+$cells expressed Foxp3. CD4$^+$CD25$^-$ T cells were incubated in a 96-well plate (1×10^4 per well) with 2×10^3 of CD11c$^+$ cells, 0.5 μg ml^{-1} of anti-CD3 antibody and the indicated number of CD4$^+$CD25$^+$ T cells for 48 h. T-cell proliferation was determined as ^{3}H-thymidine incorporation during the last 12 h of culture.

Statistical analysis

Comparative analyses of the data were performed by the Student's *t*-test, using SPSS statistical software (SPSS Japan Inc., Tokyo, Japan). $P<0.05$ was considered as a significant difference.

CONFLICT OF INTEREST

The authors declare no conflict of interest.

ACKNOWLEDGEMENTS

This work was supported in part by a grant-in-aid for the 3rd Term Comprehensive 10-year Strategy for Cancer Control from the Ministry of Health, Labour and Welfare of Japan, by grants-in-aid for Cancer Research from the Ministry of Health, Labour and Welfare of Japan and by the program for promotion of Foundation Studies in Health Science of the National Institute of Biomedical Innovation (NIBIO) and by Kobayashi Foundation for Cancer Research. H Hara and T Udagawa are awardees of a Research Resident Fellowship from the Foundation for Promotion of Cancer Research. We thank Vical Incorporated for providing the DMRIE/DOPE liposome.

1 Rabinovich GA, Gabrilovich D, Sotomayor EM. Immunosuppressive strategies that are mediated by tumor cells. *Annu Rev Immunol* 2007; **25**: 267–296.
2 Wrzesinski C, Restifo NP. Less is more: lymphodepletion followed by hematopoietic stem cell transplant augments adoptive T-cell-based anti-tumor immunotherapy. *Curr Opin Immunol* 2005; **17**: 195–201.
3 Hu HM, Poehlein CH, Urba WJ, Fox BA. Development of antitumor immune responses in reconstituted lymphopenic hosts. *Cancer Res* 2002; **62**: 3914–9391.
4 Dummer W, Niethammer AG, Bacccala R, Lawson BR, Wagner N, Reisfeld RA *et al.* T cell homeostatic proliferation elicits effective antitumor autoimmunity. *J Clin Invest* 2002; **110**: 185–192.
5 Borrello I, Sotomayor EM, Rattis FM, Cooke SK, Gu L, Levitsky HI. Sustaining the graft-versus-tumor effect through posttransplant immunization with granulocyte-macrophage colony-stimulating factor (GM-CSF)-producing tumor vaccines. *Blood* 2000; **95**: 3011–3019.
6 Kobayashi A, Hara H, Ohashi M, Nishimoto T, Yoshida K, Ohkohchi N *et al.* Allogeneic MHC gene transfer enhances an effective antitumor immunity in the early period of autologous hematopoietic stem cell transplantation. *Clin Cancer Res* 2007; **13**: 7469–7479.
7 Pfeffer LM, Dinarello CA, Herberman RB, Williams BR, Borden EC, Bordens R *et al.* Biological properties of recombinant α-Interferons: 40th anniversary of the discovery of interferons. *Cancer Res* 1998; **58**: 2489–2499.
8 Belardelli F, Ferrantini M, Proietti E, Kirkwood JM. Interferon-alpha in tumor immunity and immunotherapy. *Cytokine Growth Factor Rev* 2002; **13**: 119–134.
9 Santini SM, Lapenta C, Santodonato L, D'Agostino G, Belardelli F, Ferrantini M. IFN-alpha in the generation of dendritic cells for cancer immunotherapy. *Handb Exp Pharmacol* 2009; **188**: 295–317.
10 Ferrantini M, Capone I, Belardelli F. Dendritic cells and cytokines in immune rejection of cancer. *Cytokine Growth Factor Rev* 2008; **19**: 93–107.
11 Hara H, Kobayashi A, Yoshida K, Ohashi M, Ohnami S, Uchida E *et al.* Local interferon-α gene therapy elicits systemic immunity in a syngeneic pancreatic cancer model in hamster. *Cancer Sci* 2007; **98**: 455–463.
12 Hara H, Kobayashi A, Narumi K, Kondoh A, Yoshida K, Nishimoto T *et al.* Intratumoral interferon-α gene transfer enhances tumor immunity after allogeneic hematopoietic stem cell transplantation. *Cancer Immunol Immunother* 2009; **58**: 1007–1021.
13 Narumi K, Kondoh A, Udagawa T, Hara H, Goto N, Ikarashi Y *et al.* Administration route-dependent induction of antitumor immunity by interferon-alpha gene transfer. *Cancer Sci* 2010; **101**: 1686–1694.
14 Rodriguez EG. Nonviral DNA vectors for immunization and therapy: design and methods for their obtention. *J Mol Med* 2004; **82**: 500–509.
15 Ohtani H. Focus on TILs: prognostic significance of tumor infiltrating lymphocytes in human colorectal cancer. *Cancer Immunity* 2007; **7**: 4–13.
16 Garcia CA, Wang H, Benakanakere MR, Barrett E, Kinane DF, Martin M. c-Jun controls the ability of IL-12 to induce IL-10 production from human memory CD4$^+$ T cells. *J Immunol* 2009; **183**: 4475–4482.
17 Pasare C, Medzhitov R. Toll pathway-dependent blockade of CD4$^+$CD25$^+$ T-cell-mediated suppression by dendritic cells. *Science* 2003; **299**: 1033–1036.

18 Curiel TJ, Coukos G, Zou L, Alvarez X, Cheng P, Mottram P *et al.* Specific recruitment of regulatory T cells in ovarian carcinoma fosters immune privilege and predicts reduced survival. *Nat Med* 2004; **10**: 942–949.
19 Lai G, Zhang N, van der Touw W, Ding Y, Ju W, Bottinger EP *et al.* Epigenetic regulation of Foxp3 expression in regulatory T cells by DNA methylation. *J Immunol* 2009; **182**: 259–273.
20 Grivennikov S, Karin E, Terzic J, Mucida D, Yu GY, Vallabhapurapu S *et al.* IL-6 and Stat3 are required for survival of intestinal epithelial cells and development of colitis-associated cancer. *Cancer Cell* 2009; **15**: 103–113.
21 Asavaroengchai W, Kotera Y, Mule JJ. Tumor lysate-pulsed dendritic cells can elicit an effective antitumor immune response during early lymphoid recovery. *Proc Natl Acad Sci USA* 2002; **99**: 931–936.
22 Morgan RA, Dudley ME, Wunderlich JR, Hughes MS, Yang JC, Sherry RM *et al.* Cancer regression in patients after transfer of genetically engineered lymphocytes. *Science* 2006; **314**: 126–129.
23 Aoki K, Barker C, Danthinne X, Imperiale MJ, Nabel GJ. Efficient generation of recombinant adenoviral vectors by Cre-lox recombination *in vitro*. *Mol Med* 1999; **5**: 224–231.
24 Ohashi M, Yoshida K, Kushida M, Miura Y, Ohnami S, Ikarashi Y *et al.* Adenovirus-mediated interferon α gene transfer induces regional direct cytotoxicity and possible systemic immunity against pancreatic cancer. *Br J Cancer* 2005; **93**: 441–449.
25 Nakayama E, Uenaka A. Effect of *in vivo* administration of Lyt antibodies. *J Exp Med* 1985; **161**: 345–355.

Immunology Letters 144 (2012) 33–40

Contents lists available at SciVerse ScienceDirect

Immunology Letters

journal homepage: www.elsevier.com/locate/immlet

Real-time *in vivo* cellular imaging of graft-*versus*-host disease and its reaction to immunomodulatory reagents

Takahiro Yamazaki[a], Kazunori Aoki[a], Yuji Heike[b], Sung-Won Kim[b], Takahiro Ochiya[c], Takako Wakeda[b], Robert M. Hoffman[d,e], Yoichi Takaue[b,g], Hitoshi Nakagama[f], Yoshinori Ikarashi[a,h,*]

[a] *Division of Gene and Immune Medicine, National Cancer Center Research Institute, 5-1-1, Tsukiji, Chuo-ku, Tokyo 104-0045, Japan*
[b] *Department of Hematology and Hematopoietic Stem Cell Transplantation, National Cancer Center Hospital, Japan*
[c] *Division of Molecular and Cellular Medicine, National Cancer Center Research Institute, Japan*
[d] *AntiCancer, Inc., 7917 Ostrow Street, San Diego, CA 92111, United States*
[e] *Department of Surgery, University of California San Diego, 200 West Arbor Drive, San Diego, CA 92103-8220, United States*
[f] *Division of Cancer Development System, National Cancer Center Research Institute, Japan*
[g] *Institute for Research, St. Luke's International Hospital, Akashi-cho, Chuo-ku, Tokyo104-8560, Japan*
[h] *Central Animal Division, National Cancer Center Research Institute, Japan*

ARTICLE INFO

Article history:
Received 28 December 2011
Received in revised form 2 March 2012
Accepted 4 March 2012
Available online 15 March 2012

Keywords:
In vivo cellular imaging
GFP
Allogeneic hematopoietic stem cell transplantation
Graft-*versus*-host disease
Immunomoduratory drug

ABSTRACT

Visualizing the *in vivo* dynamics of individual donor cells after allogeneic hematopoietic stem cell transplantation (HSCT) will enable deeper understanding of the process of graft-*versus*-host disease (GVHD) and graft-*versus*-leukemia (GVL). In this study, using non-invasive *in vivo* fluorescence imaging of the ear pinna, we successfully visualized green fluorescent protein (GFP) donor cells at the single cell level in the skin. This imaging model enabled visualization of the movement of GFP cells into blood vessels in real time after allogeneic HSCT. At day 1, a few donor cells were detected, and the movement of donor cells in blood vessels was readily observed at day 4. Early donor cell infiltration into non-lymphoid tissue was increased by treatment with croton oil, as an inflammatory reagent. Treatment with dexamethasone, as an anti-inflammatory reagent, suppressed donor cell infiltration. The *in vivo* cellular fluorescence imaging model described here is a very useful tool for monitoring individual donor cells in real-time and for exploring immunomodulatory reagents for allogeneic HSCT, as well as for understanding the mechanism of GVHD.

1. Introduction

Allogeneic hematopoietic stem cell transplantation (HSCT) is an effective cell-therapy for hematological malignancies [1–3]. Donor immune cells in the graft promote the elimination of leukemic cells known as graft-*versus*-leukemia (GVL). However, donor T cells, which recognize major and minor histocompatibility antigenic disparity between donor and host, trigger host-tissue damage, termed graft-*versus*-host disease (GVHD), which is a potentially fatal adverse reaction of allogeneic HSCT [2–5]. The control of GVHD is one of the major challenges in clinical oncology. *In vivo* imaging techniques using green fluorescent protein (GFP) or luciferase transgenic mice as donors have been used to visualize the dynamics of donor immune cells after allogeneic HSCT. Imaging has demonstrated that donor T cells initially migrate into secondary lymphoid tissues where they undergo activation and proliferation and enter target tissues, such as the liver, gastrointestinal tract and skin [6–11].

In vivo fluorescence imaging has been widely used for whole-body visualization in real time and multiple colors [12–20]. Further, single cell imaging can visualize lymphocyte trafficking in lymphatic and blood vessels [21,22], as well as cell-to-cell interaction in lymph nodes [23,24]. In a GVHD mouse model, donor cells were tracked at the single-cell level *in vivo* [7,25].

In this study, using *in vivo* fluorescence imaging with cellular resolution, we evaluated the effects of immunomodulatory drugs on donor-cell migration at the single-cell level in non-lymphoid tissue such as ear pinna. It was thus possible to assess the effects of the drug, and have a control, in the same animal when the drug was painted on one ear pinna with the other serving as a control.

2. Materials and methods

2.1. Mice

Female C57BL/6-Tg (CAG-EGFP) mice (termed B6-GFP-Tg, H-$2^{b/b}$), ubiquitously expressing enhanced green fluorescence protein [26], and (C57BL/6NCrSlc × DBA/2CrSlc) F_1 (termed BDF1, H-$2^{b/d}$)

* Corresponding author at: Central Animal Division, National Cancer Center Research Institute, 5-1-1, Tsukiji, Chuo-ku, Tokyo 104-0045, Japan.
Tel.: +81 3452 2511x4452; fax: +81 3248 1631.
E-mail addresses: yikarash@gan2.ncc.go.jp, yikarash@ncc.go.jp (Y. Ikarashi).

0165-2478/$ – see front matter © 2012 Elsevier B.V. All rights reserved.
doi:10.1016/j.imlet.2012.03.004

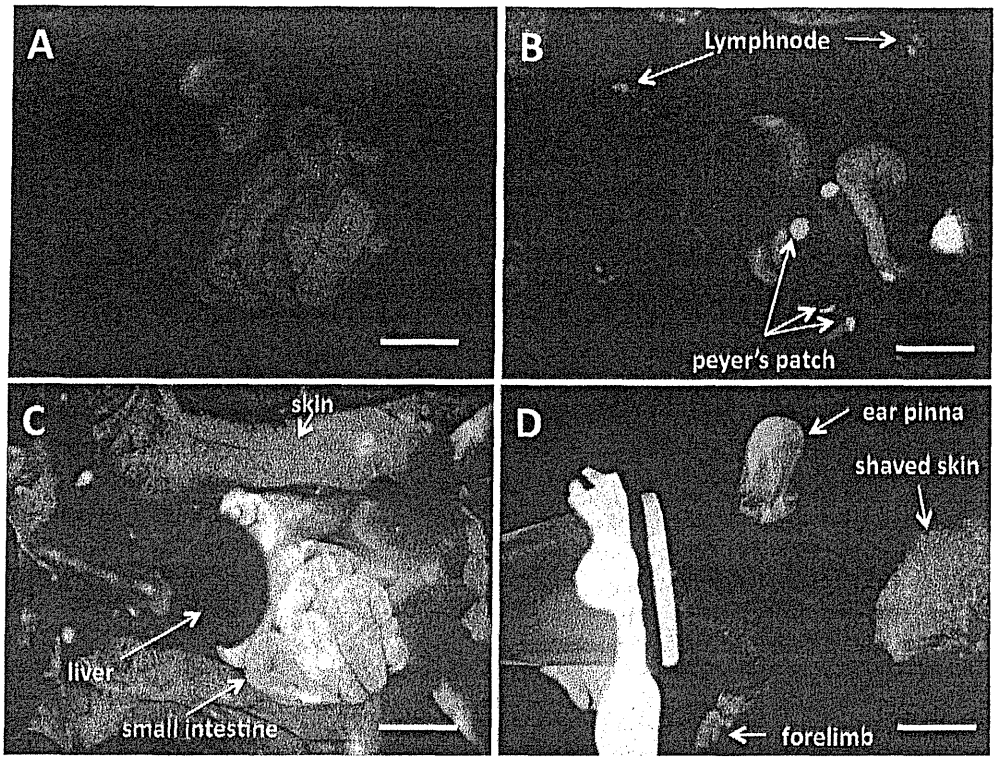

Fig. 1. *In vivo* fluorescence imaging of donor cells in opened mice after allogeneic HSCT. Spleen and bone marrow cells from B6-GFP-Tg donor mice were injected intravenously into BDF1 mice. (A–C) Mice were sacrificed and opened. GFP donor cells in whole body were visualized with the OV110 Small Animal Imaging System (A: control, B: 1 day, C: 14 days). (D) Thirty five days after transplantation, shaved mice were anesthetized and imaged with the OV110. Arrows indicate GFP+ cells in organs.

mice, were purchased from Japan SLC, Inc. (Hamamatsu, Japan). All mice were maintained in specific pathogen-free conditioned animal facilities at the National Cancer Center Research Institute. Mice between 8 and 12 weeks of age were used for all transplantation experiments. Animal studies were carried out according to the Guideline for Animal Experiments and approved by the committee for ethics of animal experimentation at the National Cancer Center.

2.2. Allogeneic HSCT mice model and treatment with immunomoduratory reagents

A mixture of 5×10^7 spleen cells and 5×10^6 bone marrow cells from B6-GFP-Tg mice was injected intravenously *via* the tail vein into untreated BDF1 mice as described previously [27,28]. Croton oil, used as an inflammatory regent, and dexamethasone, used as an anti-inflammatory reagent, were obtained from Sigma–Aldrich (St. Louis, MO). At 3 h or 7 days after allogeneic HSCT, the mice were painted on the right ear pinna with croton oil (acetone 1 μl/20 μl) or dexamethasone (acetone 0.5 μg/20 μl), respectively. As a control, the same mice were painted on the left ear pinna with 20 μl acetone alone.

2.3. Variable magnification in vivo fluorescence imaging

The OV110 Small Animal Imaging System (Olympus, Tokyo, Japan) with a cooled charge-coupled device CCD color camera and a GFP-bandpass filter, was used for non-invasive imaging from macro to micro [13]. The mice were anesthetized with isoflurane by inhalation, and sequentially imaged for the GFP donor cells in the ear pinna and shaved skin. Exposure times were optimized and identical for each experiment. Video was acquired at 10 frames/s. All images and video were obtained with OV110 software. To assess the effects of drugs on donor cell infiltration after allogeneic HSCT, GFP donor cell infiltration in the ear pinna was quantitatively analyzed. GFP donor cells in the ear pinna were initially counted and calculated as the number of donor cells per mm^2. At later stages after transplantation, the fluorescence intensity of GFP was calculated with OV110 software. To avoid contamination of autofluorescence from hair, images were obtained from the hairless areas in the ear pinna. When video of the movement of GFP cells in the blood vessels was made, hair in the ear pinna was removed by epilation to avoid autofluorescence.

2.4. Donor cell imaging in tissue sections and immunofluorescence staining

Tissues were fixed with 4% paraformaldehyde in PBS at 4 °C for 1 h followed by transfer into 10% sucrose in PBS for 12–24 h and 20% sucrose in PBS over 12 h. The tissues were embedded into an O.C.T. compound (Miles Laboratory, IN), and quickly frozen in cold isopentane. For immunofluorescence staining, the frozen block was cut into 5 μm thick sections with a cryostat (Sakura Finetek Japan, Tokyo, Japan). The sections were air-dried and incubated with blocking solution (5% normal goat serum and 1% bovine serum albumin in PBS) for 30 min and then incubated overnight at 4 °C with anti-CD3ε (500A2, eBioscience, San Diego, CA). Sections were then incubated with Alexa Fluor 594-conjugated goat anti-rat IgG antibody (invitrogen) for 1 h at room temperature. After each incubation, sections were washed with PBS containing 0.01% Triton X. Sections were mounted with VECTASHIELD with DAPI

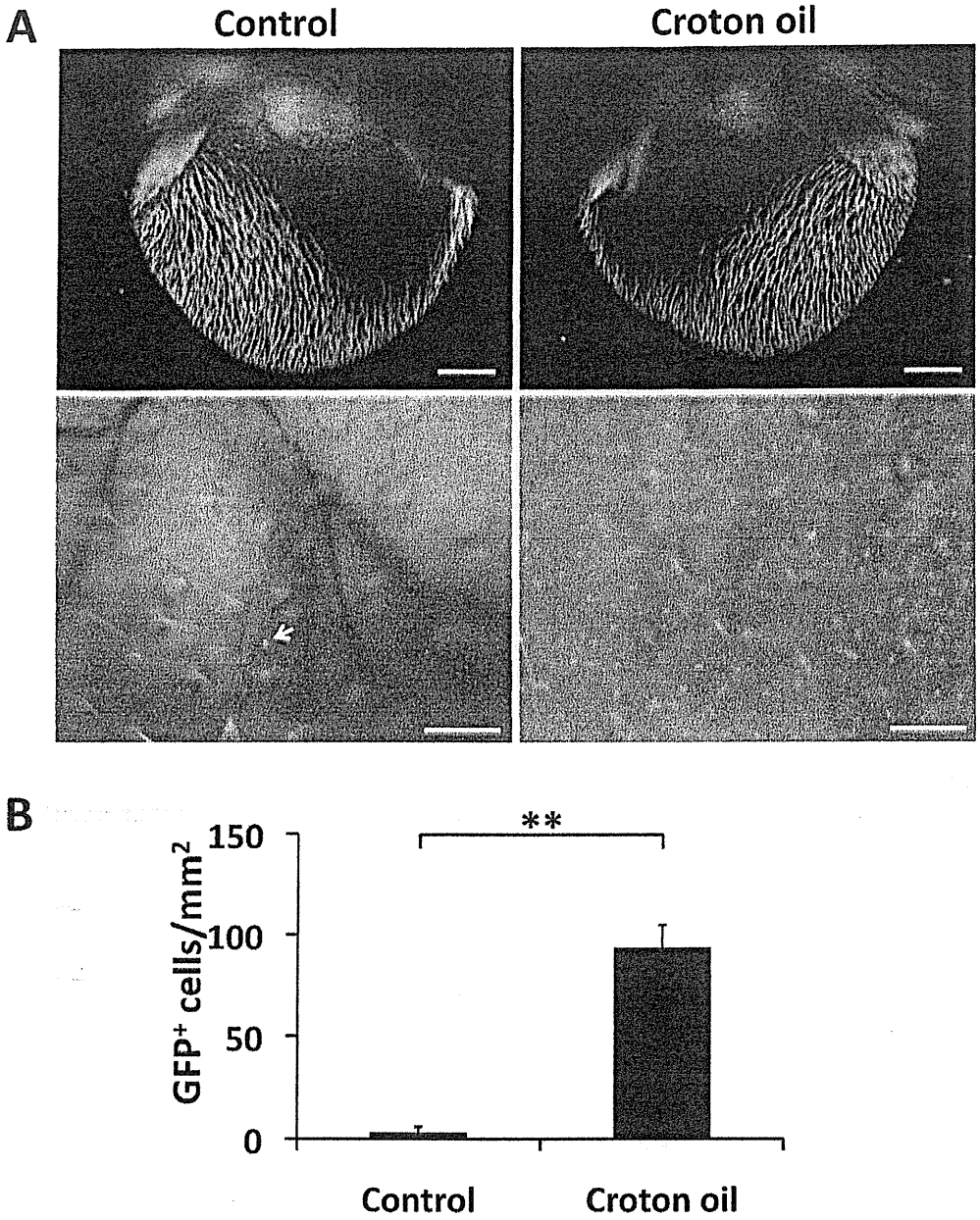

Fig. 2. Quantitative *in vivo* fluorescence imaging of donor cells in the ear pinna and the effects of inflammatory agents. (A) At 3 h after transplantation, croton oil (right panels) and acetone alone as a control (left panels), were painted on right and left ears, respectively. At day 1, GFP donor cells in the ear pinna were imaged. Low magnification images are in upper panels (scale bar, 2 mm) and high magnification images are in lower panels (scale bar, 250 μm.). Data are representative of 7 mice. (B) At day 1 after transplantation, GFP cells were counted in the ear pinna with high magnification and the number of GFP cells per 1 mm^2 was calculated. The data were from 13 fields from 5 mice and show mean ± SD. $^{**}p < 0.01$. Arrow indicates GFP+ cell.

(Vector Laboratories, Inc., Burlingame, CA). The sections were observed under fluorescence microscopy (Eclipse E1000, Nikon, Tokyo, Japan) equipped with a QICAM FAST1394 CCD camera (QImage, Surrey, BC, Canada) and Meta Morph software (Universal Imaging Corp., Buckinghamshire, UK). In the tissue sections, the number of donor cells was quantitated by manually counting GFP cells.

2.5. Statistical analysis

The statistical significance of differences between experimental groups was determined using the Student's *t*-test.

3. Results

3.1. Fluorescence imaging of donor cells after allogeneic HSCT

Using a fluorescence macro–microscopic imaging system (OV110), we could clearly visualize GFP donor cell localization in mice with open abdomens (Fig. 1A–C). GFP fluorescence was easily distinguished from orange autofluorescence in the gastrointestinal tract (Fig. 1). Similar to previous reports [7], donor cells immediately localized to secondary lymphoid tissues and then infiltrated into the whole body in the allogeneic HSCT recipients. We readily detected GFP cells in the shaved skin, ear pinna and forelimb at day 35 after transplantation (Fig. 1D). GFP donor cells were also

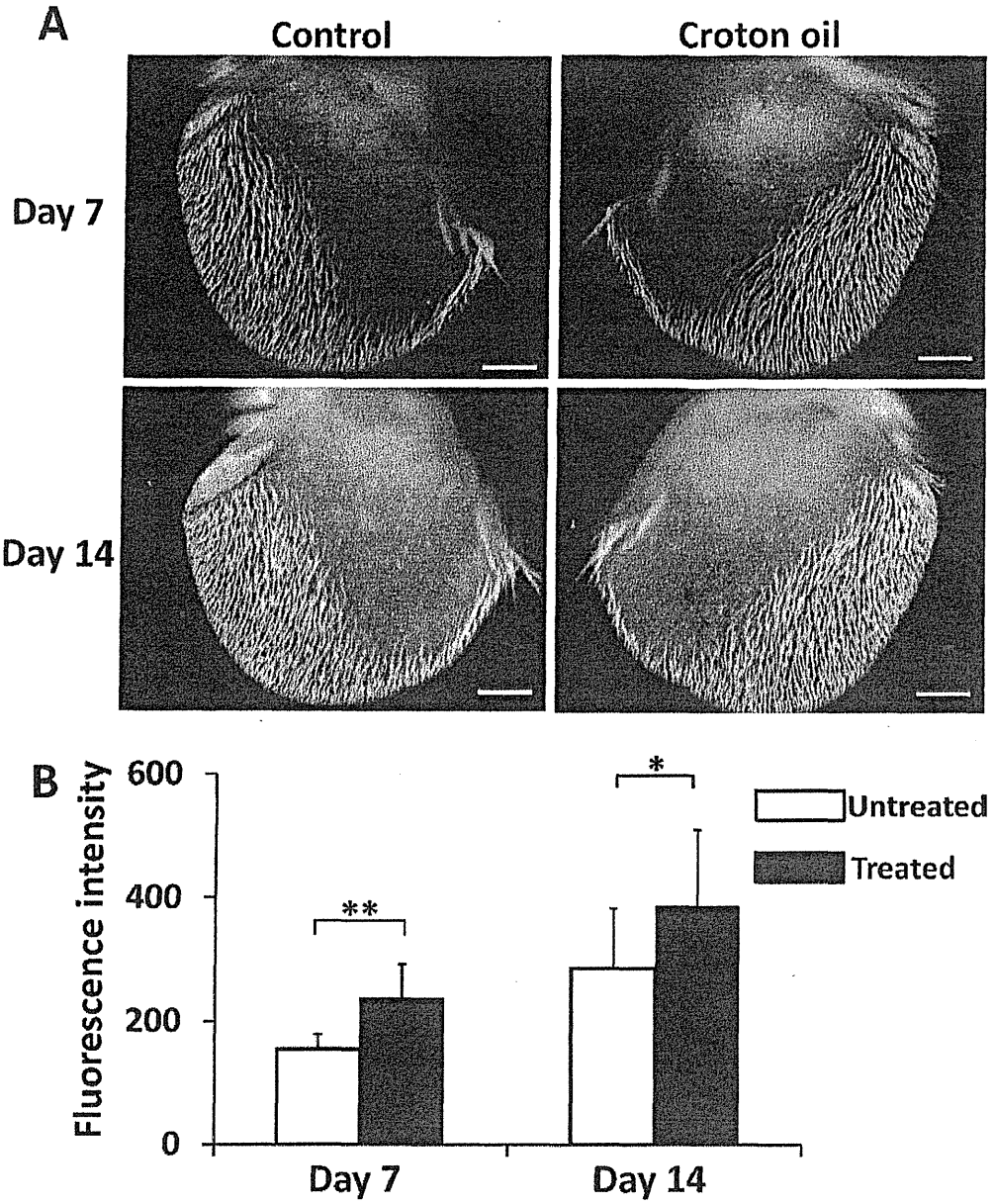

Fig. 3. *In vivo* imaging of exacerbation of donor cell infiltration by treatment with croton oil. (A) At 3 h after transplantation, croton oil (right panels) and acetone alone as control (left panels) were painted on right and left ears, respectively. At 7 (upper panels) and 14 (lower panels) days after transplantation, GFP donor cells in the ear pinna were imaged with the OV110 (scale bar, 2 mm.). Data are representative of 8–12 mice. (B) Fluorescence intensity of GFP was measured with the OV110 software. The data were from 8 mice and show mean ± SD. $^{*}p < 0.05$, $^{**}p < 0.01$.

detected in the liver, small intestine, lymphnode and Peyer's patch at the single-cell level in the dissected mice (data not shown).

3.2. *Non-invasive in vivo fluorescence imaging of donor cells in the ear pinna at the single-cell level after allogeneic HSCT*

To sequentially monitor donor cell infiltration after transplantation in the same mouse, we imaged the donor cells in the ear pinna. We determined whether donor cells could be non-invasively imaged in the ear pinna at the single-cell level. At day 1 after transplantation, donor cells were detectable at that site (Fig. 2A, lower left panel). Further, we could observe the movement of GFP donor cells into the blood vessels in the ear pinna. At day 4, GFP donor cells rapidly flowing, rolling or attaching to the vessels in the ear pinna were observed (supplemental video 1). These results indicate that it is possible to non-invasively monitor the dynamics of donor cells in the skin at the single-cell level.

3.3. *Imaging the efficacy of immunomodulatory agents*

We assessed whether non-invasive *in vivo* fluorescence imaging would be useful for screening immunomodulatory drugs for GVHD in the skin, which is a major target for GVHD. First, we tested the effect of croton oil as an inflammation stimulator after allogeneic HSCT. At 3 h after transplantation, the mice were painted with croton oil on the right ear with the left ear serving as a control. At day 1 after transplantation, increased infiltration of donor cells was clearly observed at high magnification in the ear pinna treated with croton oil (Fig. 2A). Moreover, it was possible to count GFP cells in the field and calculate the number of

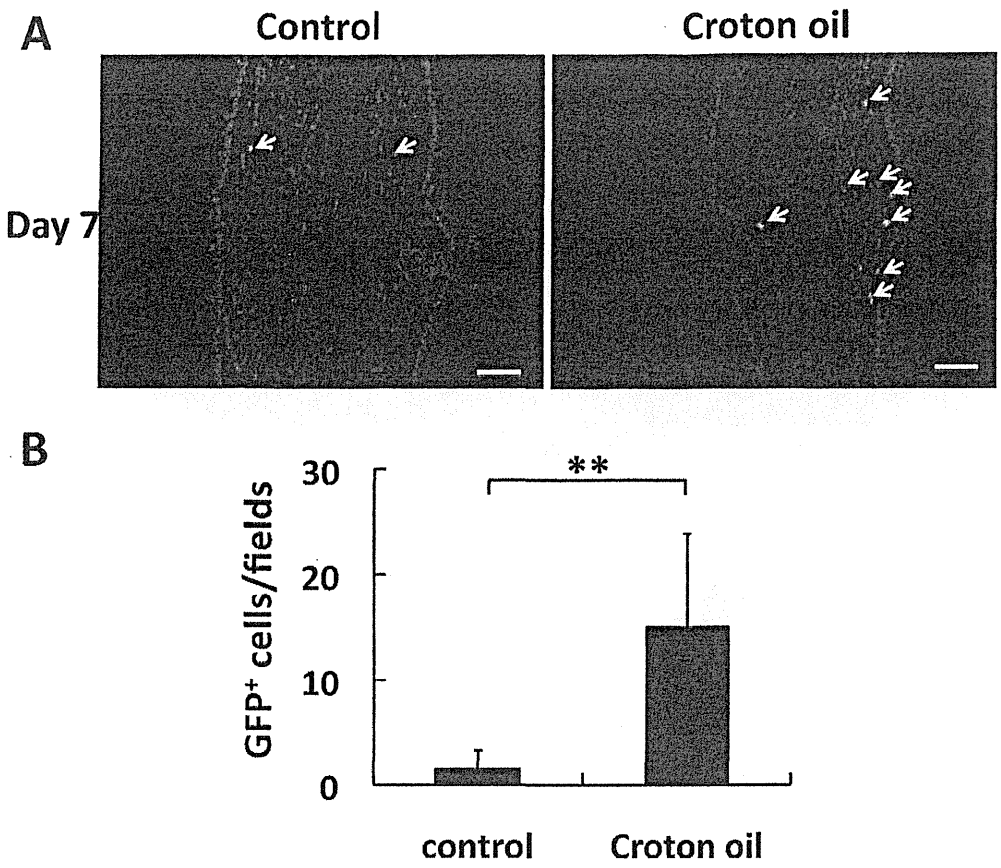

Fig. 4. Quantitative analysis of donor cell infiltration in frozen sections. (A) At 3 h after transplantation, croton oil (right panels) and acetone alone as control (left panels) were painted on right and left ears, respectively. At day 7 after transplantation, GFP cells in the frozen tissue sections were observed by fluorescence microscopy (scale bar, 50 μm.). (B) At day 7 after transplantation, GFP cells were counted in the frozen sections. Data were from 20 fields from 3 mice and show mean ± SD. $^{**}p < 0.01$.

donor cells per area. At day 1, a few GFP cells were observed in the control ear pinna, whereas approximately 90 GFP cells per mm^2 pinna accumulated in the ear after treatment with croton oil (Fig. 2B).

At 7 and 14 days after transplantation, donor cell infiltration was obviously increased in the ear pinna by treatment with croton oil (Fig. 3A). Since counting the number of infiltrating donor cells with the OV110 was difficult, due to the accumulation of many donor cells in the ear pinna, we calculated the fluorescence intensity per area using OV110 software. The analysis showed that donor cell infiltration was significantly increased in croton-oil-treated ear pinna at 7 and 14 days after transplantation (Fig. 3B). To validate the quantification of donor cell infiltration using *in vivo* imaging, we compared it with the conventional method of counting the number of GFP cells in frozen sections. Similar to *in vivo* imaging, GFP cells were found to be significantly increased in the frozen sections from croton-oil-treated tissue (Fig. 4). These results indicated that non-invasive *in vivo* fluorescence imaging is able to evaluate the effects of immunomodulatory drugs on donor-cell infiltration after allogeneic HSCT.

In order to determine whether anti-inflammatory drugs suppress donor-cell infiltration in allogeneic HSCT recipients, dexamethasone, as an anti-inflammatory drug, was painted on the right ear at day 7 after transplantation and monitored for alteration of donor cell infiltration (Fig. 5A). *In vivo* fluorescence imaging revealed that dexamethasone could significantly suppress donor cell infiltration at 14 days after transplantation (Fig. 5).

3.4. *Identification of infiltrating cell subsets using immunofluorescence staining*

Next, we identified the subsets of infiltrating cells. At day 7 after transplantation, $CD3^+$ and GFP cells were observed in the croton oil-treated ear pinna, using immunofluorescence staining (Fig. 6A and B). At day 14, dexamethasone treatment suppressed GFP-cell and $CD3^+$-cell infiltration in the skin (Fig. 6C and D). GFP^- $CD3^+$-cells derived from the host were also observed (Fig. 6B and C).

4. Discussion

An analysis of the *in vivo* dynamics of donor cells is useful for understanding the process of allogeneic HSCT, such as GVHD, GVL and reconstitution of hematopoietic and immune systems. *In vivo* imaging techniques are suitable for an analysis of the dynamics of donor cells after allogeneic HSCT and have revealed their migration and expansion patterns [6–11]. In the present report, we showed that a non-invasive *in vivo* macro–micro fluorescence imaging system is a very useful tool for monitoring donor cells at the single cell level and in real time, and for exploring inhibitory drugs and exacerbating factors of GVHD.

The skin is a major target tissue of GVHD and cutaneous involvement is the most frequent GVHD manifestation [4,5]. To monitor the skin after induction of GVHD, it was possible to non-invasively and sequentially visualize individual GFP donor cells in mice [3]. Further, using the ear pinna, GFP donor cells infiltrating the immunomodulatory drug-treated ear were able to be compared

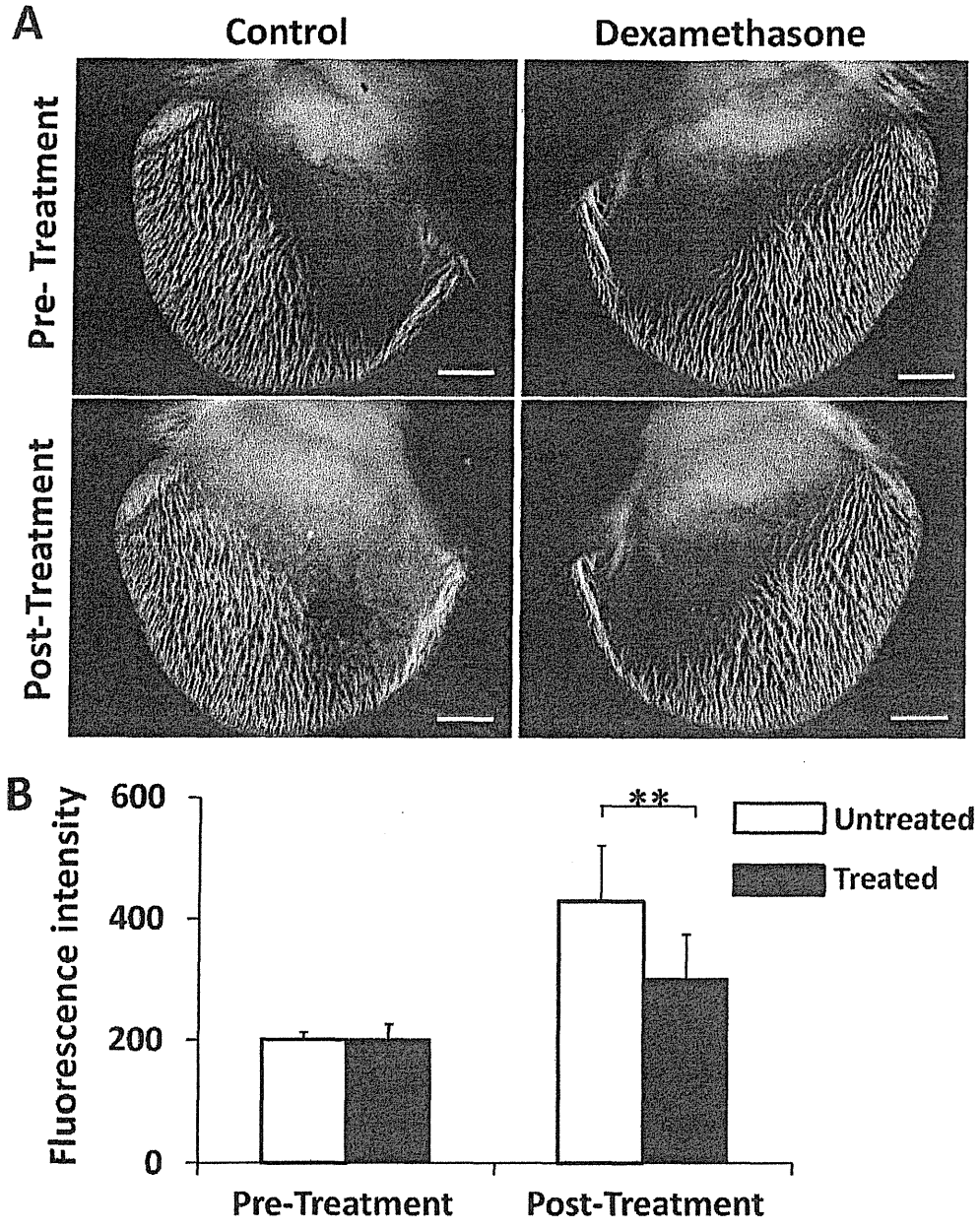

Fig. 5. The effect of dexamethasone on donor cell infiltration. (A) At 7 days after transplantation, dexamethasone (right panels) and acetone alone as control (left panels) were painted on right and left ears, respectively. Before treatment (upper panels) and at day 14 after transplantation (lower panels), GFP donor cells in the ear pinna were imaged with the OV110 (scale bar, 2 mm.). Data are representative of 8 mice. (B) Fluorescence intensity of GFP was measured with the OV110 software. The data were from 7 mice and show mean ± SD. $^{**}p < 0.01$.

with those in the untreated ear in the same animal, enabling the determination of the effects of immunomodulatory drugs for skin GVHD at the local level. It has been previously reported that donor cells could be detected in lymph nodes at 6 h [7,29]. Using fluorescence macro–microscopy, we could image individual GFP donor cells in whole ear pinna including the trafficking of donor cells in the blood vessels.

Fluorescence imaging as well as conventional methods for counting GFP cells in frozen sections revealed that GFP cell infiltration was significantly increased by croton oil. The advantages of *in vivo* fluorescence imaging are its ability to count individual GFP cells in the large area of the ear pinna and evaluate the degree of donor cell infiltration in real-time without having to make frozen sections. Moreover, we could sequentially monitor GFP cells in the same animal to compare treated and untreated ear pinna in the same mouse to evaluate the effects of drugs on skin GVHD in real time.

Regarding selectivity of donor cells recruitment, Panoskaltsis-Mortari et al. [7] reported that donor cells were observed in lymphoid tissues at 7 days after transplantation in syngeneic mice, but they are not present or present only at low levels in target tissues such as skin, liver and lung compared with allogeneic mice. Therefore, we suggest that donor cells which are observed in the skin in our report are selectively recruited.

Immunofluorescence staining analysis enabled identification of the infiltrating donor and host cell subsets in the lesions and increased our understanding of the pathogenesis of GVHD. Immunofluorescence staining revealed that at day 1 after transplantation, GFP cells detected in the ear pinna treated with croton oil were $Gr1^+$ cells, and that a large number of recipient $Gr1^+$ cells

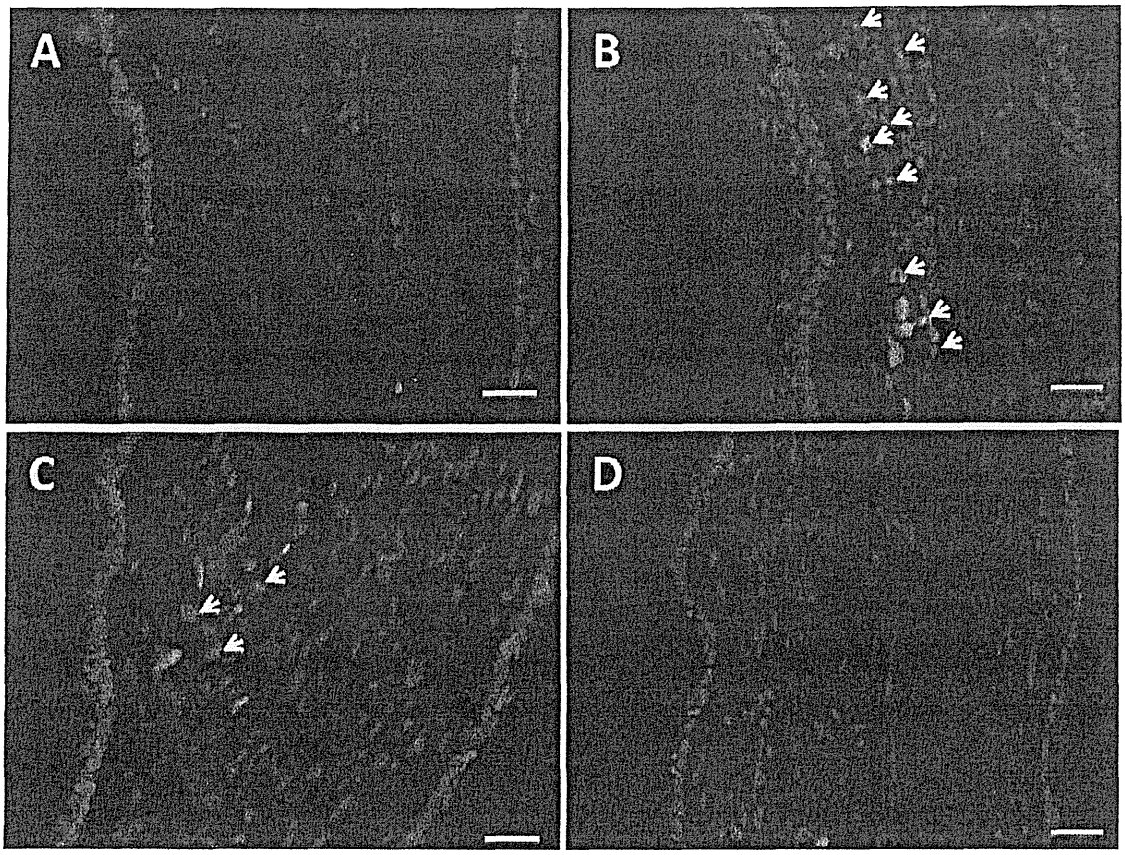

Fig. 6. Identification of infiltrating donor cell subsets using immunofluorescence staining. (A and B) At 3 h after transplantation, croton oil (B) and acetone alone as control (A) were painted on right and left ears, respectively and analyzed at day 7 after transplantation. (C and D) At day 7 after transplantation, dexamethasone (D) and acetone alone as control (C) were painted on right and left ears, respectively and analyzed at day 14 after transplantation. (A–D) Frozen sections of ear pinna were stained with CD3 monoclonal antibody and GFP and $CD3^+$ cells were observed by fluorescence microscopy (scale bar, 100 μm). Arrows indicate GFP $CD3^+$ cells (donor T cells). Data are representative of 3 mice.

(GFP^- cells) also infiltrated (data not shown). Croton oil stimulation is known to induce neutrophil accumulation [30,31]; therefore early recruitment of both donor- and recipient-type $Gr1^+$ cells could be elicited by croton oil stimulation rather than allogeneic responses. Activated neutrophils produce several chemkines such as CXCL9, CXCL10 and CXCL11 which attract CXCR3-expressing T cells [32–34]. Furthermore, on day 3 after transplantation, CXCL10 and CXCL11 produced in target tissues, directed the early recruitment of activated CXCR3-expressing donor T cells [35]. Our results showed that increased donor cell infiltration was observed in the ear pinna treated with croton oil after transplantation. We suggest that increased donor cell infiltration could be dependent not only on inflammatory responses by croton oil, but on allogeneic responses as well. Immunofluorescence staining of CD3, infiltrating T cells showed they were both donor and recipient. In this study, we used non-myeloablative allogeneic HSCT mouse models. Recipient immune cells were not depleted by conditioning; thus, recipient T cells might be involved in the lesions [22]. Treatment with corticosteroid alleviates skin GVHD, which was demonstrated by fluorescence imaging in real time.

In conclusion, non-invasive and single cell *in vivo* imaging using a fluorescence macro–microscope is very useful for drug screening for early- and late-stage GVHD in real time.

Acknowledgments

This work was supported in part by a Grant-in-Aid for scientific research from the Japan Society for the Promotion of Science, National Cancer Center Research and Development Fund, a Grant-in-Aid from the Suzuken Memorial Foundation and a Grant-in-Aid from the Advanced Clinical Research Organization.

Appendix A. Supplementary data

Supplementary data associated with this article can be found, in the online version, at doi:10.1016/j.imlet.2012.03.004.

References

[1] Horowitz MM, Gale RP, Sondel PM, Goldman JM, Kersey J, Kolb HJ, et al. Graft-versus-leukemia reactions after bone marrow transplantation. Blood 1990;75:555–62.
[2] Appelbaum FR. Haematopoietic cell transplantation as immunotherapy. Nature 2001;411:385–9.
[3] Welniak LA, Blazar BR, Murphy WJ. Immunobiology of allogeneic hematopoietic stem cell transplantation. Annu Rev Immunol 2007;25:139–70.
[4] Ferrara JL, Levine JE, Reddy P, Holler E. Graft-versus-host disease. Lancet 2009;373:1550–61.
[5] Shlomchik WD. Graft-versus-host disease. Nat Rev Immunol 2007;7:340–52.
[6] Negrin RS, Contag CH. In vivo imaging using bioluminescence: a tool for probing graft-versus-host disease. Nat Rev Immunol 2006;6:484–90.
[7] Panoskaltsis-Mortari A, Price A, Hermanson JR, Taras E, Lees C, Serody JS, et al. In vivo imaging of graft-versus-host-disease in mice. Blood 2004;103:3590–8.
[8] Stelljes M, Hermann S, Albring J, Köhler G, Löffler M, Franzius C, et al. Clinical molecular imaging in intestinal graft-versus-host disease: mapping of disease activity, prediction, and monitoring of treatment efficiency by positron emission tomography. Blood 2008;111:2909–18.
[9] Taylor PA, Ehrhardt MJ, Lees CJ, Panoskaltsis-Mortari A, Krieg AM, Sharpe AH, et al. TLR agonists regulate alloresponses and uncover a critical role for donor APCs in allogeneic bone marrow rejection. Blood 2008;112:3508–16.

[10] Beilhack A, Schulz S, Baker J, Beilhack GF, Wieland CB, Herman EI, et al. In vivo analyses of early events in acute graft-versus-host disease reveal sequential infiltration of T-cell subsets. Blood 2005;106:1113–22.
[11] Nguyen VH, Zeiser R, Dasilva DL, Chang DS, Beilhack A, Contag CH, et al. In vivo dynamics of regulatory T-cell trafficking and survival predict effective strategies to control graft-versus-host disease following allogeneic transplantation. Blood 2007;109:2649–56.
[12] Hoffman RM. The multiple uses of fluorescent proteins to visualize cancer in vivo. Nat Rev Cancer 2005;5:796–806.
[13] Yamauchi K, Yang M, Jiang P, Xu M, Yamamoto N, Tsuchiya H, et al. Development of real-time subcellular dynamic multicolor imaging of cancer-cell trafficking in live mice with a variable-magnification whole-mouse imaging system. Cancer Res 2006;66:4208–14.
[14] Hoffman RM, Yang M. Whole-body imaging with fluorescent proteins. Nat Protoc 2006;1:1429–38.
[15] Yamauchi K, Yang M, Jiang P, Yamamoto N, Xu M, Amoh Y, et al. Real-time in vivo dual-color imaging of intracapillary cancer cell and nucleus desformation and migration. Cancer Res 2005;65:4246–52.
[16] Hoffman RM. In vivo real-time imaging of nuclear-cytoplasmic dynamics of dormancy, proliferation and death of cancer cells. APMIS 2008;116:716–29.
[17] Yamauchi K, Yang M, Hayashi K, Jiang P, Yamamoto N, Tsuchiya H, et al. Induction of cancer metastasis by cyclophosphamide pretreatment of host mice: an opposite effect of chemotherapy. Cancer Res 2008;68:516–20.
[18] Yang M, Li L, Jiang P, Moossa AR, Penman S, Hoffman RM. Dual-color fluorescence imaging distinguishes tumor cells from induced host angiogenic vessels and stromal cells. Proc Natl Acad Sci U S A 2003;100:14259–62.
[19] Yang M, Reynoso J, Jiang P, Li L, Moossa AR, Hoffman RM. Transgenic nude mouse with ubiquitous green fluorescent protein expression as a host for human tumors. Cancer Res 2004;64:8651–6.
[20] Hasegawa A, Hayashi K, Kishimoto H, Yang M, Tofukuji S, Suzuki K, et al. Color-coded real-time cellular imaging of lung T-lymphocyte accumulation and focus formation in a mouse asthma model. J Allergy Clin Immunol 2010;125:461–8.
[21] Miller MJ, Wei SH, Cahalan MD, Parker I. Autonomous T cell trafficking examined in vivo with intravital two-photon microscopy. Proc Natl Acad Sci U S A 2003;100:2604–9.
[22] Mempel TR, Scimone ML, Mora JR, von Andrian UH. In vivo imaging of leukocyte trafficking in blood vessels and tissues. Curr Opin Immunol 2004;16:406–17.
[23] Stoll S, Delon J, Brotz TM, Germain RN. Dynamic imaging of T cell-dendritic cell interaction in lymph nodes. Science 2002;296:1873–6.
[24] Mempel TR, Henrickson SE, Von Andrian UH. T-cell priming by dendritic cells in lymph nodes occurs in three distinct phases. Nature 2004;427:154–9.
[25] Chakraverty R, Côté D, Buchli J, Cotter P, Hsu R, Zhao G, et al. An inflammatory checkpoint regulates recruitment of graft-versus-host reactive T cells to peripheral tissues. J Exp Med 2006;203:2021–31.
[26] Okabe M, Ikawa M, Kominami K, Nakanishi T, Nishimune Y. 'Green mice' as a source of ubiquitous green cells. FEBS Lett 1997;407:313–9.
[27] Ikarashi Y, Matsumoto Y, Omata S, Fujiwara M. Recipient-derived T cells participate in autoimmune-like hepatic lesions induced by graft-versus-host reaction. Autoimmunity 1995;20:121–7.
[28] Kuwatani M, Ikarashi Y, Iizuka A, Kawakami C, Quinn G, Heike Y, et al. Modulation of acute graft-versus-host disease and chimerism after adoptive transfer of in vitro-expanded invariant Valpha14 natural killer T cells. Immunol Lett 2006;106:82–90.
[29] Taylor PA, Ehrhardt MJ, Lees CJ, Tolar J, Weigel BJ, Panoskaltsis-Mortari A, et al. Insights into the mechanism of FTY720 and compatibility with regulatory T cells for the inhibition of graft-versus-host disease (GVHD). Blood 2007;110:3480–8.
[30] Mizgerd JP, Bullard DC, Hicks MJ, Beaudet AL, Doerschuk CM. Chronic inflammatory disease alters adhesion molecule requirements for acute neutrophil emigration in mouse skin. J Immunol 1999;162:5444–8.
[31] Komatsu N, Waki M, Sue M, Tokuda C, Kasaoka T, Nakajima M, et al. Heparanase expression in B16 melanoma cells and peripheral blood neutrophils before and after extravasation detected by novel anti-mouse heparanase monoclonal antibodies. J Immunol Methods 2008;331:82–93.
[32] Gasperini S, Marchi M, Calzetti F, Laudanna C, Vicentini L, Olsen H, et al. Gene expression and production of the monokine induced by IFN-gamma (MIG), IFN-inducible T cell alpha chemoattractant (I-TAC), and IFN-gamma-inducible protein-10 (IP-10) chemokines by human neutrophils. J Immunol 1999;162:4928–37.
[33] Molesworth-Kenyon SJ, Oakes JE, Lausch RN. A novel role for neutrophils as a source of T cell-recruiting chemokines IP-10 and Mig during the DTH response to HSV-1 antigen. J Leukoc Biol 2005;77:552–9.
[34] Seiler P, Aichele P, Bandermann S, Hauser AE, Lu B, Gerard NP, et al. Early granuloma formation after aerosol Mycobacterium tuberculosis infection is regulated by neutrophils via CXCR3-signaling chemokines. Eur J Immunol 2003;33:2676–86.
[35] Wysocki CA, Burkett SB, Panoskaltsis-Mortari A, Kirby SL, Luster AD, McKinnon K, et al. Differential roles for CCR5 expression on donor T cells during graft-versus-host disease based on pretransplant conditioning. J Immunol 2004;173:845–54.

KOKUYO セホ-60DM